

JGR Space Physics

RESEARCH ARTICLE

10.1029/2019JA026903

Special Section:

Long-term changes and Trends in the Middle and Upper Atmosphere

Key Points:

- There is a suggestion of an increase in hydrogen emission intensity between two solar maxima, with a caveat that it is a limited data set
- The apparent increase in intensity is counter to previous observations of the response of hydrogen emissions to changes in solar activity
- The apparent increase in intensity is likely of larger magnitude than would be predicted due to greenhouse gas increases

Correspondence to:

S. M. Nossal, nossal@physics.wisc.edu

Citation:

Nossal, S. M., Mierkiewicz, E. J., Roesler, F. L., Woodward, R. C., Gardner, D. D., & Haffner, L. M. (2019). Geocoronal hydrogen emission variation over two solar cycles. *Journal* of Geophysical Research: Space Physics, 124. https://doi.org/10.1029/ 2019JA026903

Received 29 APR 2019 Accepted 25 SEP 2019 Accepted article online 18 NOV 2019

Geocoronal Hydrogen Emission Variation Over Two Solar Cycles

S. M. Nossal¹ , E. J. Mierkiewicz² , F. L. Roesler¹, R. C. Woodward³ , D. D. Gardner⁴ , and L. M. Haffner^{2,5}

¹Department of Physics, University of Wisconsin-Madison, Madison, WI, USA, ²Department of Physical Sciences, Embry-Riddle Aeronautical University, Daytona Beach, FL, USA, ³Department of Physics/Astronomy, University of Wisconsin Oshkosh, Fond du Lac Campus, Fond du Lac, WI, USA, ⁴Lunar and Planetary Laboratory, University of Arizona, Tucson, AZ, USA, ⁵Space Science Institute, Boulder, CO, USA

Abstract Ground-based hydrogen Balmer-α observations from Northern midlatitudes span multiple solar cycles, facilitating investigation of decadal scale variations, including natural variability in the hydrogen response to solar geophysical changes. Here we present a reanalysis of ground-based hydrogen emission observations from the early 1990s and their comparison with observations obtained in 2000-2001 in the context of the extended Northern Hemisphere midlatitude geocoronal hydrogen emission data set. This work suggests an increase in hydrogen emission intensity between the solar-maximum period of 1990-1991 (Solar Cycle 22) and the near-solar-maximum period of 2000-2001 (Solar Cycle 23), with the caveat that this is a limited data set and that there are calibration uncertainties discussed in this paper. Solar activity was higher during the earlier solar maximum period. Thus, the apparent increase in intensity is counter to previous observations from midlatitudes in which the observed intensity increases with higher solar activity. This increase was also not seen in comparison of intensities from three solar minima periods. Further, the apparent increase in intensity is also likely of larger magnitude than model simulations would predict due to increases in methane and carbon dioxide. We will discuss the reanalysis and recalibration of the 1990-1991 observations using current analysis approaches and the interpretation of these observations in the context of observations and modeling of hydrogen variation over different time scales. The detailed review of the calibration procedures has also provided insights to guide design of future observations.

Plain Language Summary Atomic hydrogen is a key constituent of the thermosphere and exosphere, the uppermost region of the Earth's atmosphere. Hydrogen in this region is a by-product of molecules at lower altitudes that contain hydrogen such as water vapor and methane, two of the greenhouse gases most important to the energy balance of the Earth. The 11-year solar cycle is a major source of natural variability in the upper atmosphere. Here we present observations of geocoronal hydrogen emissions (~400 km and above) taken by ground-based Fabry-Perot instruments at Wisconsin and at the Kitt Peak, Observatory in Arizona. These observations span two solar cycles and suggest an increase in the geocoronal hydrogen emission intensity between the 1990–1991 solar maximum (Solar Cycle 22) and the 2000–2001 near-solar-maximum (Solar Cycle 23) periods, with the caveat that this is a limited data set and there are calibration uncertainties. Solar activity was higher during the earlier solar maximum period. The apparent increase in intensity is counter to previous observations from midlatitudes in which the observed intensity increases with higher solar activity. Further, the apparent increase in intensity is also likely of larger magnitude than model simulations would predict due to increases in methane and carbon dioxide.

1. Introduction

Long-term data records are essential for understanding natural variability and human impacts on our climate system (see e.g., Intergovernmental Panel on Climate Change, 2013). Numerical models predict a whole atmosphere response to increases in greenhouse gases with predicted impacts extending through the upper thermosphere (Qian et al., 2011; Roble & Dickinson, 1989; Solomon et al., 2018). Satellite drag measurements are consistent with thermospheric cooling, a predicted signature in the upper atmosphere of increases in atmospheric carbon dioxide (Emmert, 2015; Emmert et al., 2004). Upper atmospheric

©2019. American Geophysical Union. All Rights Reserved.

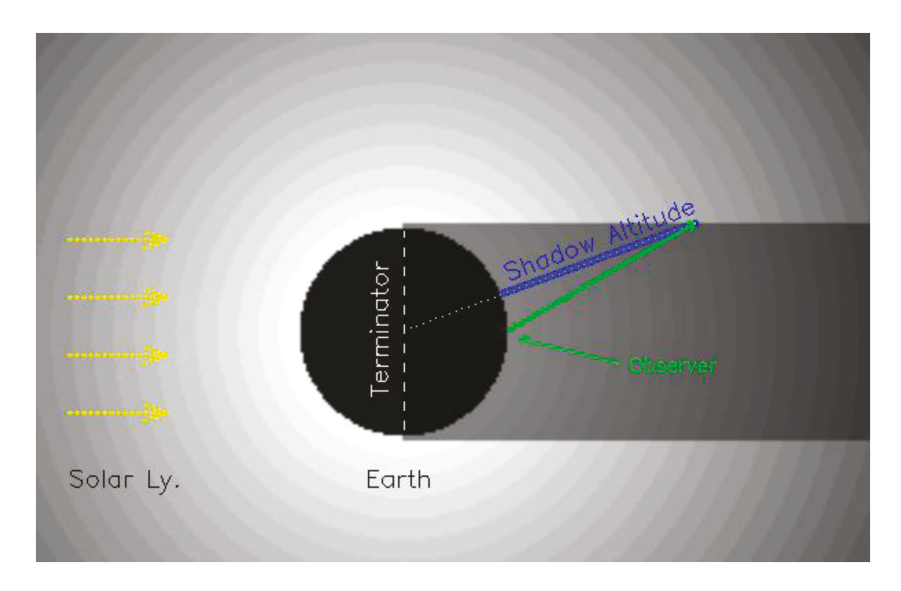


Figure 1. (reprinted from Gardner, Mierkiewicz, Roesler, Harlander, et al., 2017) illustrates how the shadow altitude is defined. The shadow altitude is the radial distance from the surface of the Earth to the location at which the observational line of sight intersects the Earth's shadow for solar Lyman- β radiation. The radius of this shadow is approximately 100 km larger than that of the Earth's due to the absorption in the upper atmosphere of the solar Lyman- β radiation. Please see text for further details.

constituent concentrations, including atomic hydrogen, are also expected to change, but acquiring historical long-term data records of these constituents is particularly challenging due to the need for remote sensing.

Atomic hydrogen is a key constituent in the near-space thermosphere and exosphere (Chamberlin & Hunten, 1987). Hydrogen charge exchanges with ions in the plasmasphere (Krall et al., 2018) and is a byproduct of lower altitude constituents containing hydrogen such as methane and water vapor, two species with large influence on the radiative balance of the Earth's atmosphere (Brasseur & Solomon, 2005). As the lightest element, hydrogen's relatively longer mean free path enables it to be more globally mixed compared with species at lower attitudes.

Hydrogen is predicted and has been observed to respond to the 11-year solar cycle, a major source of natural variability in the Earth's upper atmosphere. Multiple numerical and empirical modeling studies (Anderson et al., 1987; Nossal et al., 2012, 2016; Qian et al., 2018; Tinsley et al., 1986) predict higher hydrogen densities in the upper thermosphere during solar minimum conditions. Both the National Research Laboratory Mass-Spectrometer-Incoherent-Scatter 00 (NRLMSISE-00; Picone et al., 2002) and the National Center for Atmospheric Research Whole Atmosphere Community Climate Model-eXtended (WACCM-X; Liu et al., 2018) predict about an order of magnitude higher hydrogen density in the upper thermosphere at solar minimum compared with during solar maximum conditions [see Figure 2 in Qian et al., 2018].

Ground-based Fabry-Perot observation of the geocoronal hydrogen Balmer- α (656.274 nm) emission has been one of the principal remote sensing techniques for studying geocoronal hydrogen (~400 km and above; Mierkiewicz, 2019). The Balmer- α emission from atomic hydrogen in the thermosphere and exosphere arises primarily due to excitation by solar Lyman- β (102.572 nm) radiation. The shadow altitude is the viewing geometry parameter with the greatest impact on the column emission intensity and is defined as the radial distance from the surface of the Earth to the location at which the observational line of sight intersects the Earth's shadow [see Figure 1 and Section 3]. Ground-based Fabry-Perot Interferometers observe an integrated column of the geocoronal Balmer- α emission with most of the emission arising from the base of the illuminated portion of the column, that is, near the shadow altitude.

The geocoronal Balmer- α emission is directly excited by the solar Lyman- β radiation and arises from the transitions along the $3P_{3/2}$ to $2S_{1/2}$ and the $3P_{1/2}$ to $2S_{1/2}$ fine structure paths of the hydrogen Balmer- α line (see e.g., Mierkiewicz et al., 2012). Additionally, there is contribution to the Balmer- α signal from cascade excitation whereby higher-energy solar Lyman line radiation excites the electron in the hydrogen atom to



energy levels higher than the n=3 state followed by cascade transitions of the electron back to the n=3 level. This process results in Balmer- α emission along all seven of the fine structure paths from the n=3 to n=2 levels of the hydrogen atom resulting in an approximate 4–5% cascade contribution to the total hydrogen Balmer- α emission intensity (Mierkiewicz et al., 2012; Roesler et al., 2014) that is depended on shadow altitude (Gardner, Mierkiewicz, Roesler, Nossal, & Haffner, 2017).

Bishop et al. (2001) provide a review and assessment of the contribution to the geocoronal hydrogen Balmer- α emission from excitation mechanisms other than the resonance fluorescent scattering described above. They consider Balmer- α emission associated with the recombination of H⁺ and e, the excitation by e + H collisional impacts in the upper atmosphere and interplanetary medium, and the energetic neutral atoms generated in the ring current. They conclude that there is an upper limit of approximately 1 Rayleigh for the Balmer- α emission that can be attributed to excitation mechanisms other than resonance fluorescent scattering (Bishop et al., 2001).

Ground-based Fabry-Perot observations from midlatitudes indicate that the *integrated* hydrogen Balmer-α column emission is higher during solar maximum conditions (Nossal et al., 2012, 2008, 2004). The Balmer-α emission arises primarily due to excitation by Lyman-β (102.6 nm) radiation from the Sun. There are few high-resolution measurements of the solar Lyman-β line profile leading to uncertainty in knowledge of the change in solar excitation flux over the solar cycle; however, extrapolation from solar minimum measurements (Warren et al., 1998) leads to estimates of the Lyman-β flux higher at solar maximum, (see discussion by Bishop et al., 2001, 2004). Additionally, Qian et al. (2018) show through theoretical studies that the distribution of hydrogen with altitude in the thermosphere is predicted to change over the course of the solar cycle, likely due to complex dynamical processes. Observations by the GUVI instrument on the TIMED satellite (Qin & Waldrop, 2016) also show a solar cycle variation in the global hydrogen Lyman-α observations, with the retrieved hydrogen exobase density higher during solar minimum conditions. Ground-based Fabry-Perot observations of the hydrogen Balmer-α column emission intensity over Arecibo, however, show solar cycle variation in the emission only at low shadow altitudes with intensities higher during solar minimum (Kerr et al., 2001a), opposite to what has been observed in our midlatitude observations from Wisconsin and Arizona. Kerr et al. (2001b) also report the suggestion of an increase in the brightness of their hydrogen emission measurements over the period of 1984 to 1994.

As is the case for hydrogen-containing constituents throughout the atmosphere, upper thermospheric atomic hydrogen is predicted to respond to anthropogenic increases in greenhouse gases. Ehhalt (1986) first postulated an increase in exospheric hydrogen of about 30% due to increases in stratospheric water vapor resulting from a doubling of tropospheric methane. In their seminal study of the impacts of greenhouse gases on the upper atmosphere, Roble and Dickinson (1989) used a one-dimensional version of the NCAR Thermosphere Ionosphere Mesosphere Electrodynamics General Circulation Model to show that thermospheric temperatures were expected to cool and the densities of upper atmospheric species were predicted to change in response to simulations involving greenhouse gas doubling, specifically carbon dioxide and methane. They attributed the ~50% increase in upper thermospheric atomic hydrogen to the doubling of methane at the lower boundary of the model.

Using an updated version of the one-dimensional model used by Roble and Dickinson (1989) that extends downward into the stratosphere, Nossal et al. (2016) ran simulation experiments to separately investigate the effects of carbon dioxide and methane doubling, as well as doubling of both species together, during both solar minimum and maximum conditions. They found that both carbon dioxide cooling and methane increases to the source species were predicted to lead to increases in upper thermospheric hydrogen densities and that this increase was predicted to be of larger magnitude during solar minimum conditions. Over decadal time scales, the predicted impacts of the solar cycle were of larger magnitude than the predicted increases due to greenhouse gas doubling. To put these numerical experiments into context, historical increases in methane and carbon dioxide are about 150% and 40%, respectively, since 1750 (Intergovernmental Panel on Climate Change, 2013) and are within a few percent over the time scale of a solar cycle. The rate of change of atmospheric methane concentrations has been more variable than has that of carbon dioxide (NOAA Global Greenhouse Gas Network; https://www.esrl.noaa.gov/gmd/ccgg/).

Observations from northern midlatitudes of the Balmer α emission from atomic hydrogen span multiple solar cycles, facilitating investigation of decadal scale variations, including natural variability in the

hydrogen response to solar geophysical changes. Here we present results from reanalysis of ground-based hydrogen emission observations from the early 1990s taken with a Fabry-Perot at the Pine Bluff, WI observatory. We also compare these observations to those taken earlier in the 1970s and 1980s, presented in Nossal et al. (1993), but which have not been reanalyzed and reviewed and so have larger uncertainty. Comparison of the 1990-1991 observations (Solar Cycle 22) with those taken in 2000-2001 (Solar Cycle 23) suggests an increase in hydrogen emission intensity between these two near-solar maximum periods, with the caveat that this is a limited data set and there remain uncertainties in the calibration. This apparent increase in intensity was not present in comparison of observations of the hydrogen column emission intensity from three solar minimum periods (Nossal et al., 2008). The Solar Cycle 23 observations (F10.7 134 to 163) were taken with the Wisconsin H-alpha Mapper Fabry-Perot (WHAM) annular-summing Fabry-Perot instrument from Kitt Peak, AZ, during winter 2000-2001 and with a second annular-summing Fabry-Perot from Pine Bluff, WI, during February 2000. The Solar Cycle 22 observations (F10.7 181 to 232) were taken with the pre-WHAM Fabry-Perot when it was at the Pine Bluff, WI, observatory. We will discuss the reanalysis and recalibration of the solar cycle 22 observations using current analysis approaches and the interpretation of these observations in the context of observations and modeling of hydrogen variation over different time scales. The detailed review of the calibration procedures has also provided insights to guide design of future observations to facilitate comparisons of variability over multiple time scales, including long-term comparisons.

2. Ground-Based Hydrogen Balmer-Alpha Emission Observations

The observations presented here were taken with three ground-based double-etalon Fabry-Perot spectrometers, each coupled to a pointing and tracking siderostat. Fabry-Perot Spectrometers offer the advantages of simultaneously offering high throughput and resolution (Roesler, 1974). Fabry-Perot spectrometers are particularly advantageous for observing faint, diffuse, line source emissions such as the Geocoronal Hydrogen Balmer-alpha emission line (656.3 nm) as well as for observing hydrogen Balmer-alpha emissions from the Galactic Interstellar Medium (Roesler et al., 1995).

2.1. . "Pre-WHAM" Scanning Fabry-Perot

The "pre-WHAM" Fabry-Perot used for the solar cycle 22 solar maximum observations during the early 1990s was a scanning Fabry-Perot that sequentially scanned through a spectral range. An aperture limited the photon collection to the center annulus of the Fabry-Perot interference pattern, and photons were detected using a photomultiplier tube. Photons were collected during equal spectral intervals in wave number by measuring the wave number interval using a Michelson Interferometer as reference (Roesler, 1974). The etalons in the "pre-WHAM" Fabry-Perot were later used in the Wisconsin H-alpha Mapper Fabry-Perot. The resolution ($\lambda/\Delta\lambda$) of the "pre-WHAM" Fabry-Perot was approximately 25,000, and geocoronal observations were made with integration times of approximately 10 min. Further details about these observations, including sample spectra, are in Nossal et al. (1993).

The "pre-WHAM" Fabry-Perot instrument was located at the Pine Bluff Observatory near Cross Plains, WI, at the time of the solar cycle 22 solar maximum observations presented here (43.08°N, 89.67°W). Previously, the instrument had been located at the Stoughton, WI, Physical Sciences Laboratory.

2.2. . Wisconsin H-Alpha Mapper ("WHAM") Annular-Summing Fabry-Perot

Most of the Solar Cycle 23 observations presented here were taken with the Wisconsin H-alpha Mapper ("WHAM") Fabry-Perot when it was located at the Kitt Peak Observatory near Tucson, Arizona (31.96°N, 111.60°W). The WHAM instrument uses the same etalons as did the "pre-WHAM" Fabry-Perot but utilized the advances of a Charged Coupled Device (CCD) imager rather than photomultiplier detection. The resolution of the WHAM instrument is ~25,000, and it is coupled to a pointing and tracking siderostat.

The Fabry-Perot interference pattern is imaged onto the CCD and converted to a spectrum using annular-summing analysis in which equal-area annuli correspond to equal spectral intervals when measured in wave number increments. The advantages of the annular-summing technique include that photons are collected in all spectral intervals simultaneously and that the quantum efficiency of the CCD Camera is higher than that for the photomultiplier, thus increasing the signal to noise and shortening the integration time of the observation (Coakley et al., 1996).

The primary purpose of the WHAM instrument is to make an all-sky map of Galactic hydrogen Balmer-alpha emissions as a probe of the warm ionized component of our Galaxy's interstellar medium. WHAM was at the Kitt Peak Observatory from 1997 to 2008 where it created an all-sky map of Galactic emissions from the Northern Hemisphere (Haffner et al., 2003). In 2009 WHAM was moved to the Cerro Tololo Observatory where it has been making observations of the Southern Sky Galactic Hydrogen emissions (Haffner et al., 2010, 2016). The Galactic spectra also contain the terrestrial emission and can be used for geocoronal studies provided that there is a sufficiently large Doppler separation between the Galactic and terrestrial emission lines (Nossal et al., 2001). Additional observations have been made in low Galactic emission regions (Nossal et al., 2008) and in the zenith direction for geocoronal investigations and observations have been made of both the geocoronal Balmer- α and Balmer- β column emission intensity (Gardner, Mierkiewicz, Roesler, Nossal, & Haffner, 2017; Roesler et al., 2014).

2.3. . Higher-Resolution Annular-Summing Fabry-Perot Interferometer

The data comparison presented here also includes observations taken by a higher-resolution Fabry-Perot using the annular-summing spectroscopy technique. This instrument was used to take observations from the Pine Bluff, WI observatory, some of which were taken during the same observing period as the WHAM Solar Cycle 23 observations and are included here (Gallant et al., 2019; Mierkiewicz et al., 2012). This Fabry-Perot was coupled to a pointing and tracking siderostat as well as to a CCD Camera. The resolution of the instrument was ~85,000, sufficiently high to investigate geocoronal spectral line profiles and intensities.

2.4. . Intensity Calibration

The intensity of geocoronal hydrogen Balmer-alpha column emission observations presented here was calibrated using astronomical calibration sources. An advantage of this method is the similarity of the astronomical calibration emission to the terrestrial emission. Both the astronomical hydrogen Balmer-alpha calibration sources and the geocoronal hydrogen Balmer-alpha emission are diffuse line sources. Both also are outside of the Earth's atmosphere and so pass through the same optics.

The NGC7000 nebula, also called the North American Nebula (NAN), is the primary calibration source that has been used by Wisconsin observers for both calibration of the geocoronal hydrogen Balmer-alpha observations and Galactic interstellar hydrogen emission observations (Scherb, 1981). The patch of NAN used for our intensity calibration is centered at a Galactic longitude of 85.6° and a Galactic latitude of -0.72° (right ascension 20h 57m 59s and declination +44d 34′ 50″ in J2000 coordinates). Additionally, the portion of the Barnard's Loop nebula (hereafter referred to as "R8," Galactic longitude 212.31° and Galactic latitude of -15.72°; right ascension 05h 54m 3.39s and declination -6.07° in J2000 coordinates) was used as a calibration source during times of the year when the NAN was not visible in the night sky (Nossal et al., 1993). An 0.8° patch of the North American was calibrated using standard stars (Scherb, 1981) and was found to be 850 \pm 50 Rayleighs. The North American Nebular calibration of the 1.0° field of view used by the WHAM instrument was estimated to be 800 R \pm 10%. Using a series of masks, Mierkiewicz extended this calibration to other fields of view (Mierkiewicz et al., 2006). The North American Nebular calibration of the 1.4° field of view used by the Pine Bluff high-resolution instrument was calculated to be ~650 Rayleighs using alternating observations of NAN and the geocorona with a stopped-down field of view (Mierkiewicz et al., 2006).

Details regarding the calibration and analysis of the WHAM geocoronal observations are described in Mierkiewicz et al. (2006) and Nossal et al. (2008, 2006). Analysis of the Pine Bluff high-resolution observations is described in Mierkiewicz (2002) and Mierkiewicz et al. (2006, 2012). The reanalysis of the 1990–1991 observations (Nossal et al., 1993) is discussed below.

3. Reanalysis Strategy

We reanalyzed the observations taken with the scanning Fabry-Perot at the Pine Bluff Observatory in the winter of 1990–1991. This effort involved reviewing the notes in the log book to identify sky conditions and confirm pointing directions as well as using our current analysis programs, including recalculation of the shadow altitude. We have most of the original spectra in digital form and used the Voigt-fit spectral fitting code to refit the original geocoronal and nebular calibration spectra.



VoigtFit is a one-dimensional parameter estimation code developed by one of us (Woodward) for spectral fitting. It uses the Levenburg-Marquardt algorithm to fit multiple Gaussian, Lorentz, and/or Voigt profiles to a spectrum. For the present work, the most useful of its features are the convolution of an empirical instrumental profile with the fit, and the linking of line centers of lines with known offsets, to reduce the number of free parameters. We then recalibrated the geocoronal observations and reevaluated our assessment of the uncertainty in the nebular calibration. We also performed sensitivity studies with an updated correction code to assess differences in tropospheric scattering contributions to the column emissions.

The shadow altitude is the viewing geometry parameter with the greatest impact on the column emission intensity and thus must be accounted for when comparing observations. The shadow altitude is defined as the radial distance from the surface of the Earth to the location at which the observational line of sight intersects the Earth's shadow for solar Lyman- β radiation. The radius of this shadow is approximately 100 km larger than that of the Earth's due to the absorption in the upper atmosphere of the solar Lyman- β radiation. Figure 1 (reprinted from Gardner, Mierkiewicz, Roesler, Harlander, et al., 2017) illustrates how the shadow altitude is defined. The shadow altitude specifies the base of the sunlit part of the atmosphere, above which hydrogen atoms are directly excited by solar Lyman- β radiation and through resonant fluorescence, produce the Balmer- α emission. There is additional contribution from excitation of hydrogen by multiple scattering of solar Lyman β into the shadow region.

We used a code derived from telescope pointing machine code of Percival (1994) to calculate the shadow altitude for both the solar cycle 21 (1990–1991) and the solar cycle 22 (2000–2001) observations. This shadow code uses the same high-precision pointing software and algorithm methodology as the telescope control systems for the WIYN 3.5 m and WHAM telescopes. The telescope pointing machine code (Percival, 1994) calculates the shadow altitude and slant path distance using rigorous vector/matrix methods for its transformations, avoiding spherical trigonometry and its associated singularity problems. A radius of 102 km larger than the Earth's radius was used when calculating the shadow altitude.

3.1. Reanalysis of the Intensity Calibration

The pre-WHAM scanning Fabry-Perot observations used a portion of the Barnard's Loop nebula ("R8"), as well as the NGC7000 (North American Nebula, NAN), for the intensity calibration of the geocoronal hydrogen emission observations. The intensity of the 0.8° field-of-view region of the NAN used for the intensity calibration was $850 \, \text{R} + / - 10\%$ (Scherb, 1981; Nossal et al., 1993) and an intensity of $130 \, \text{R} + / - 15\%$ has been used as the intensity of the R8 region used for the calibration (Nossal et al., 1993). The R8 region is present in the night sky during winter months in Madison when NAN is not observable or only at high zenith angles when tropospheric scattering uncertainties are greater. One of the principle sources of uncertainty in the intensity calibration is the uncertainty in the relative intensity determination between the region of R8 and of the NAN used for the calibrations. One of the goals of this reanalysis study was to corroborate the intensity calibration used in the original analysis of the pre-WHAM observations (Nossal et al., 1993).

There are fewer calibration spectra available for the pre-WHAM Fabry-Perot observations than is the case for the WHAM annular-summing observations. Fewer calibration spectra were taken with the scanning instrument because of the longer integration times (approximately 10 min) required compared with the time required for a WHAM nebular calibration (approximated 30–60 s). To assess sky conditions during the pre-WHAM observations, peak count rates of the nebular emission were monitored more often than were full spectral observations. Additionally, the original calibration spectra could only be located for some of the nebular observations.

We refit original calibration spectra taken with the scanning pre-WHAM Fabry-Perot instrument using the Voigt-fit spectral fitting code and calculated a "calibration factor" similar to that calculated for the WHAM observations (Nossal et al., 2008). The intensity of an overlapping geocoronal hydrogen emission line of about 1–12 R is significant in comparison to the R8 but not the NAN intensity. Thus, when fitting the R8 spectra, we accounted for the geocoronal hydrogen emission intensity. As for the geocoronal spectra, the time interval per data point was close but not uniform for the data points comprising the nebular spectra. Thus, we divided the counts in each data point by the time interval to put the data into the format of counts per second before fitting.

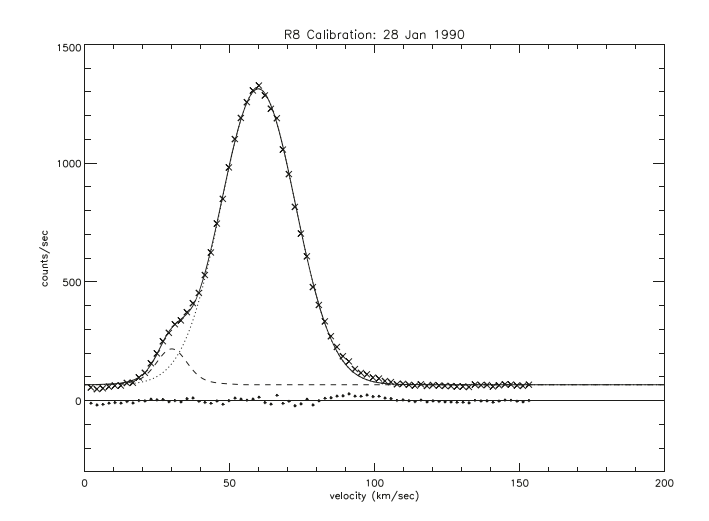


Figure 2. Sample observation by the pre-WHAM Fabry-Perot of a portion of the Barnard's Loop ("R8"), a secondary calibration source to the North American Nebula (NAN), used when NAN was not visible in the nightsky. The spectrum is plotted using a velocity scale (km/s) on the x axis versus counts per second on the y axis, with the "zero" km/s point at an arbitrary location. The spectral intervals correspond to Doppler shifts to the red to the right side of the plot. The spectrum includes contributions from both the nebular and overlapping geocoronal emission. Please see text for further details.

As illustrated in Figure 2, the overlap between the geocoronal and nebular hydrogen emission lines made it difficult to unambiguously isolate the two emission lines. We thus fit both lines together and then subtracted off the estimated geocoronal emission to calculate the R8 emission intensity. To estimate the intensity of the geocoronal hydrogen emission line that overlaps with the R8 nebular hydrogen emission line, we calculated the shadow altitude corresponding to the nebular calibration line. We used pointing coordinates corresponding to the J2000 epoch as inputs to the shadow code of Percival and calculated the corresponding shadow altitude for the time of the observation. Using this shadow information, we used the intensity versus shadow altitude dependence from the original analysis to estimate the geocoronal emission intensity in the pointing direction and at the time of the nebular observation.

To compare the variation in the nebular count rate, we defined a nebular calibration factor, assuming that an R8 intensity of 130 R +/- 15% as published in Nossal et al. (1993).

The intensity of the geocoronal line can be calculated from the nebular calibration as defined in equation (1) below (see, e.g., Nossal et al., 2008, 2006, and Mierkiewicz et al., 2006, for more information).

$$I_{geo} = I_{Neb} \frac{A_{geo}}{A_{Neb}} e^{\tau \left(sec\left(ZA_{geo}\right) - sec(ZA_{Neb})\right)} \frac{Exposure \ time_{Neb}}{Exposure \ time_{geo}}, \tag{1}$$

where

Igeo geocoronal intensity

$$\begin{split} &I_{Neb} & \text{ intensity of the nebular calibration source} \\ &A_{geo} & \text{ area of the geocoronal emission spectral profile} \\ &A_{Neb} & \text{ area of the nebular emission spectral profile} \end{split}$$

atmospheric extinction coefficient

ZA_{geo} zenith angle of the geocoronal observation

ZA_{Neb} zenith angle of the nebular observation e time_{geo} exposure time for the geocoronal observation

 $\begin{array}{ll} \text{exposure time}_{\text{geo}} & \text{exposure time for the geocoronal observation} \\ \text{exposure time}_{\text{Neb}} & \text{exposure time for the nebular observation} \end{array}$

For the reanalysis of the "pre-WHAM" observations, we used an atmospheric extinction coefficient of $\tau = 0.14$, consistent with measurements in Mierkiewicz et al. (2006).

For the photomultiplier data we plot the counts per second, and so the formula above can be reduced to that in equation (2).

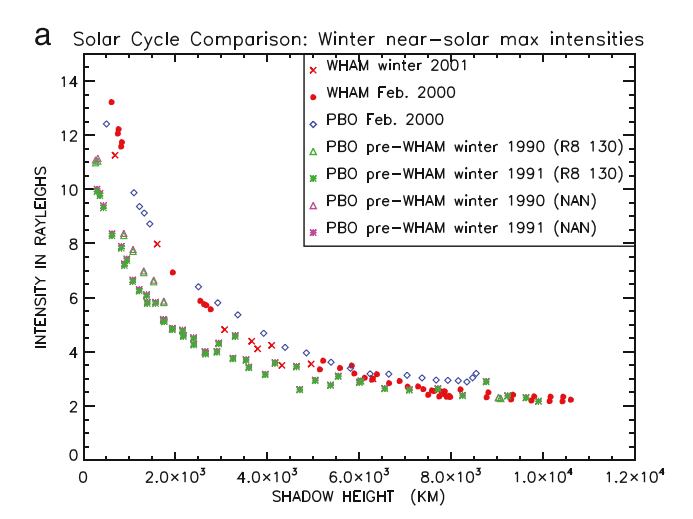
$$I_{geo} = I_{Neb} \frac{A_{geo}}{A_{Neb}} e^{\tau \left(sec\left(ZA_{geo}\right) - sec\left(ZA_{Neb}\right)\right)}$$
 (2)

To compare nebular calibration values from different spectra, we define a nebular factor as follows in equation (3).

$$F_{Neb} = I_{Neb} \frac{e^{-\tau(sec(ZA_{Neb}))}}{A_{Neb}}$$
 (3)

7

Then the intensity of the geocoronal line can be calculated as follows in equation (4).



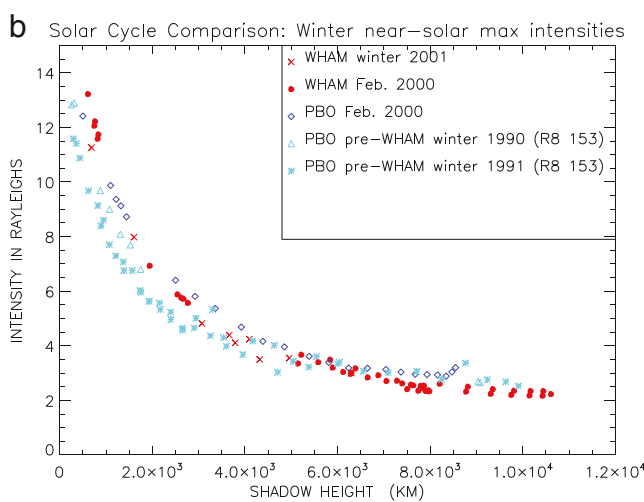


Figure 3. (a) The 2000–2001 (Solar Cycle 23) observations (F10.7 134 to 163) were taken with the WHAM Fabry-Perot instrument from Kitt Peak, AZ, during winter 2000–2001 (red symbols) and with a second Fabry-Perot from Pine Bluff, WI, during February 2000 (blue symbols). The 1990–1991 (Solar Cycle 22) observations (F10.7 181 to 232) were taken with the pre-WHAM Fabry-Perot at Pine Bluff Wisconsin. In this figure, the 1990–1991 observations have been reanalyzed using an R8 calibration value of 130 R (green symbols) and using the North American Nebula calibration (purple symbols). (b) Same as (a) except that the 1990–1991 observations have been reanalyzed using an R8 calibration value of 153 R (aqua symbols).

$$I_{geo} = F_{Neb} A_{geo} e^{\tau (sec(ZA_{geo}))}$$
 (4)

We used R8 calibration spectra taken on nights with better sky conditions as indicated by the observing log notes. We also limited the R8 spectra to those taken at zenith angles less than 60° to minimize the effects of tropospheric scattering. Using four R8 spectra from different nights, we calculated a R8 calibration factor for the 1990–1991 observations with a variation in the calculated factor of within 12%. Sky conditions, small differences in pointing, and possible instrument degradation could contribute to the variation in the calibration factor. The assumed R8 intensity of 130 Rayleighs is consistent with the calculated value for the R8 intensity using an NAN observation taken in August of 1990 during our best sky conditions.

We also used an R8 and an NAN observation taken in 1987 for Galactic investigations using the same pre-WHAM instrument when it was earlier located at the Physical Sciences Laboratory in Stoughton, WI. Calibrating this R8 spectrum with an NAN spectrum taken with the same instrument gave a value for the intensity of R8 of 153 Rayleighs. There is a possibility that there may have been a small change in the field of view of the pre-WHAM instrument when it was moved from the Stoughton, WI, location to the Pine Bluff, WI, observatory and that this change in the field of view may have contributed to the discrepancy in the R8 calibration. We further corroborated the calibration by calculating the intensity of the 0.8° patch of R8 using the WHAM Galactic map and a flux-weighing approach described in Gardner, Mierkiewicz, Roesler, Harlander, et al. (2017). The value of the intensity of R8 calculated in this manner was 129 Rayleighs with the caveat that the WHAM map observations were taken with a 1° field of view. We present the 1990-1991 observations analyzed with both the 130 and 153 R values attributed to the intensity of the R8 calibration to give a measure of the uncertainty in this calibration.

4. Results

Observations of the hydrogen Balmer- α column emission intensity taken during or near two solar maxima periods are plotted in Figures 3a and 3b. The column emission intensity is plotted as a function of shadow altitude because the shadow altitude is the viewing geometry parameter with the greatest impact on the column emission intensity. For a given shadow altitude, differences in zenith angle and hence slant path may result in intensity differences within ~1 Rayleigh (Nossal et al., 2001).

All observations in Figures 3a and 3b are from winter periods and include observations taken during morning and evening conditions. The observations were taken when the moon was not visible to avoid reflected sunlight from the moon and during our dates of best sky conditions. Winter months typically provide better sky conditions and the longest nights for observations. Further, winter comparisons minimize seasonal differences (Gallant et al., 2019). Each period of observations includes several nights. While the data represent a small number of dates for each data set, we have found that observations taken during the same observing period are consistent from night to night. The 2000–2001 (Solar Cycle 23) observations at near solar maximum conditions (F10.7 134 to 163) were taken during lower solar activity conditions compared with those taken during the solar maximum period of 1990–1991 (Solar Cycle 22; F10.7 181 to 232).

The WHAM observations plotted here were a subset taken in pointing directions toward low Galactic regions of the sky. The pre-WHAM observations were taken in the zenith direction and at times to avoid the Galactic plane. All of the observations presented here were corrected for atmospheric extinction. The



atmospheric optical thickness or extinction coefficient can be calculated using observations of a source such as an astronomical nebula taken at different zenith angles (see, e.g., Mierkiewicz et al., 2006).

It is more difficult, however, to account for the portion of the signal that arises due to scattering into the line of sight within the troposphere. We have run sensitivity simulations using a tropospheric scattering correction code. This code couples a heterogeneous geocoronal source function to a Monte Carlo radiative transfer code of Petty (2002, 2006). The top-of-the atmosphere diffuse source function of Balmeralpha emission is defined by a grid of points across the sky, determining time-dependent viewing geometry parameters for these points, and then calling the LYAO RT code of Bishop (1999) to determine the relative strength of the geocoronal hydrogen emission intensity at each point. We used the NRLMSISE-00 model (Picone et al., 2002) extended to exospheric altitudes with the Bishop (1991, 2001) evaporative analytic exosphere model (Nossal et al., 2012) as the hydrogen distribution for calculating the geocoronal source function with the lyao_rt code. This source of geocoronal Balmer-alpha emission across the sky is then coupled to the Monte Carlo code, which computes the direct (unscattered) and diffuse (scattered) contributions to the Balmer-alpha emission observed from the ground along a given line of sight. Tropospheric scattering contributions to the column emission would be expected to be greater at the Pine Bluff Observatory than at Kitt Peak due to the clearer site conditions at Kitt Peak. Simulations with our radiative transfer correction code suggest that differences in the tropospheric scattering contributions between observations from the Kitt Peak, Arizona, and Pine Bluff, Wisconsin, observatories would be within 1 Rayleigh at lower shadow altitudes and less at higher shadow altitudes. The reanalyzed 1990-1991 intensity observations as well as the intensity observations taken by the Wisconsin H-alpha Mapper Fabry-Perot have not yet been corrected for tropospheric scattering. Applying the tropospheric scattering correction code to individual data points is one of the steps that could be included in the next phase of the reanalysis to reduce the uncertainty in the relative intensity comparison.

The same observations are presented in Figures 3a and 3b, with a difference in the intensity calibration for the 1990–1991 observations. The red symbols are a subset of the 2000–2001 observations from the Wisconsin H-alpha Mapper annular-summing Fabry-Perot when it was located at the Kitt Peak Observatory (Nossal et al., 2008, 2012). The dark blue symbols are observations taken with a high-resolution annular-summing Fabry-Perot at the Pine Bluff, WI, observatory during the same observing period as when the WHAM observations were made. The green symbols in Figure 3a are the 1990–1991 observations calibrated with R8 spectra using an intensity of 130 R for the observed patch of R8, and the purple points are the same 1990–1991 observations using a calibration from with a NAN observation (850 R) taken during the summer and with the best observing conditions. In Figure 3b, the same 1990–1991 observations are calibrated with R8 observations from that period, but assuming an intensity value of 153 R for R8 (aqua symbols). In all cases the 1990–1991 observations are of lower intensity than are the 2000–2001 observations.

The intensity of all of the observations presented in this study were calibrated with nebular emissions tied to a 0.8° patch of the NAN. Figures 3a and 3b illustrate uncertainty in the determination of the intensity of the R8 secondary calibration source. The calibration of R8 intensity using R8 observations compared with an NAN observation taken from Pine Bluff, WI, with the pre-WHAM Fabry-Perot with the best sky conditions gave a value of 130 Rayleighs and was used to calibrate the data presented in Figure 3a. An R8 and an NAN observation taken in 1987 using the same pre-WHAM instrument when it was earlier located at the Physical Sciences Laboratory in Stoughton, WI, gave a value for the intensity of R8 of 153 Rayleighs. We used this intensity calibration value of 153 Rayleighs to calibrate the 1990–1991 observations plotted in Figure 3b. We believe that there is insufficient information to definitively determine which of the two calibrations of R8 is more correct, and thus, we present the 1990–1991 data analyzed with both. We present the resulting difference in retrieved geocoronal Balmer- α column emission intensity as a measure of the uncertainty in the absolute intensity calibration.

The observations taken with the higher-resolution annular-summing Fabry-Perot instrument when it was located at the Pine Bluff, WI, observatory are a subset overlapping with the two-week dark moon period when the WHAM 2000 observations were taken. Additional observations from this Pine Bluff annular-summing Fabry-Perot are shown in Mierkiewicz et al. (2012). The Balmer α column emission intensities in Figure 4 of Mierkiewicz et al. (2012) contain observations from throughout the year, and, as shown in Gallant et al. (2019), the intensity has a seasonal dependence, particularly at low shadow altitudes. To

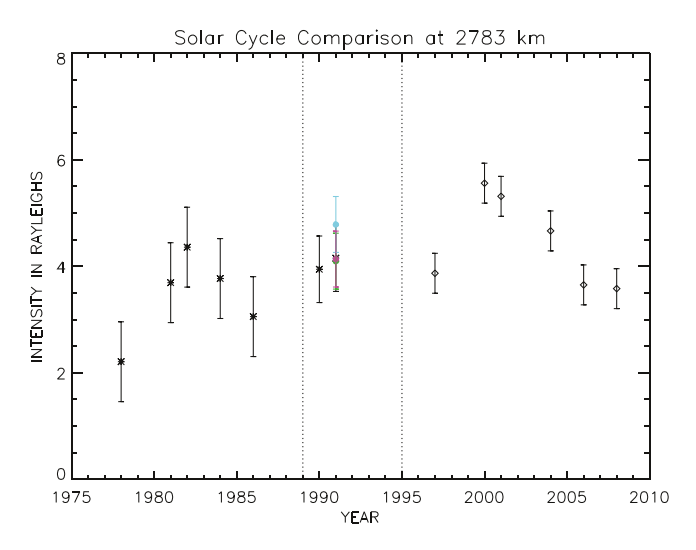


Figure 4. The extended Northern Hemisphere midlatitude geocoronal hydrogen emission data set. An intensity for a midrange shadow altitude of 2,783 km is plotted in half-year bins spanning winter conditions. The bins represent multiple spectra, in most cases from multiple nights. We have been treating the pre-WHAM and the WHAM observations as separate data sets as indicated by the right-hand dotted line. The original spectra from the 1990-1991 observations have been reanalyzed and included in the middle section of this plot. The earlier data from the 1970s and 1980s (Nossal et al., 1993) have not been reanalyzed. An intensity for a midrange shadow altitude of 2,783 km is plotted by year. Superimposed are these reanalyzed intensities for the 1991 observations at a shadow altitude of 2,783 using the value of 130 R for the R8 calibration (green circle), the calibration from the observation of the North American Nebula (purple circle), and the calibration value of 153 R for the R8 calibration (aqua circle). Error bars indicate estimates for uncertainty in the relative intensity comparison. Please see text for further details.

isolate effects other than seasonal and because sky conditions are typically best in winter, our focus for this reanalysis study is on winter observations.

Figure 4 illustrates the 1990–1991 solar maximum and 2000–2001 near solar maximum observations in the context of the extended Northern Hemisphere midlatitude geocoronal hydrogen emission data set. We have been treating the pre-WHAM and the WHAM observations as separate data sets as indicated by the dotted line. In Figure 4, an intensity for a midrange shadow altitude of 2,783 km is plotted in half-year bins spanning winter conditions. Each bin typically represents multiple nights and spectra. The solar F10.7 cm flux is included in Figure 5 for reference. A goal of the study presented here is to work toward merging the two data sets and to develop observational and analysis strategies to guide future trend studies of upper atmospheric hydrogen emissions.

The pre-WHAM observations in Figure 4 were analyzed and compared using a methodology similar to that described in Nossal et al. (1993) by which observations were taken in ratio to intensities predicted by the model of Anderson et al. (1987), and then the ratios were fit with a linear fit. This model is a Monte Carlo model coupled to a radiative transfer code that predicts ground-based column emission intensities for solar minimum, medium, and maximum conditions. Normalizing the observed intensity to the model predictions for the corresponding viewing geometry facilitated comparison without the large intensity variation with viewing geometry. Additionally, as an alternative to taking an average, this approach minimized skewing of the results due to clustering of the observations at certain solar depression angles, which occurred in some of the data sets (Nossal et al., 1993). For the data comparison, we chose to ratio all of the pre-WHAM observations to the Anderson et al. (1987) solar maximum submodel to minimize variation due to differences in the submodels. For the majority of the observations, the ratios were closest to unity for intensities compared with the solar maximum submodel, inde-

pendent of solar conditions [see Figure 6 in Nossal et al., 1993], and overall the ratios were more invariant with shadow altitude compared with when all the observations were ratioed to the solar minimum or medium Anderson et al. (1987) submodels.

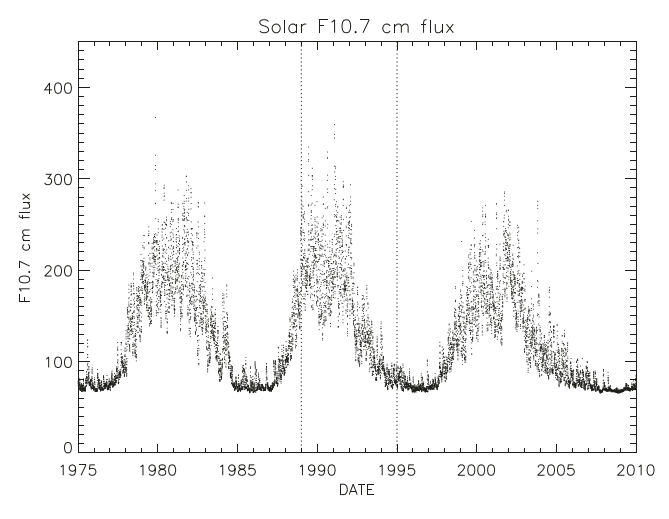


Figure 5. Daily Solar Radio F10.7 cm flux. These data were downloaded from the LASP Interactive Solar Irradiance Data Center (http://lasp.colorado.edu/lisird/data/noaa_radio_flux/).

In Figure 4, the pre-WHAM observations are taken in ratio to predictions using the Anderson et al. (1987) solar maximum submodel and then the ratio at a solar depression of 45° is determined using a linear fit to the ratios as described in Nossal et al. (1993). The pre-WHAM observed-to-model intensity ratios are then normalized to the intensity of 4.15 R, the corresponding reanalysis intensity at a solar depression of 45° for the 1991 observations. The 1991 pre-WHAM observations were taken in the zenith direction, and the corresponding shadow altitude for a solar depression of 45° was 2,783 km. This comparison at a midrange shadow altitude reduces uncertainty due to higher intensities observed at low shadow altitudes during dawn compared with intensities at the same shadow altitudes during dusk conditions (Gallant et al., 2019).

For the original analysis of the pre-WHAM data (1970s, 1980s, and 1990–1991; Nossal et al., 1993), the data bins contained observations from a half year period with the point plotted at the midpoint of the time interval. The points plotted in Figure 4 are those spanning winter months and are thus a subset of those included in Figure 6 of Nossal et al. (1993). Each bin contains multiple observations (see Figures 3a, 3b, and 6 of this paper and Figures 3, 4, 7, and 9 in Nossal et al., 1993). In some cases there are

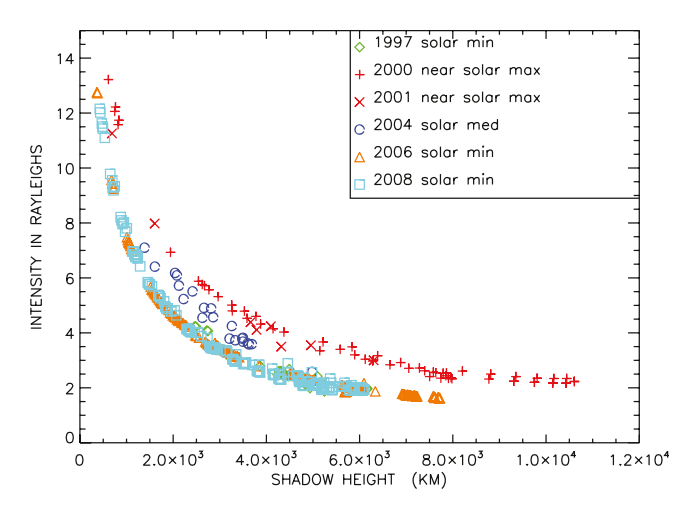


Figure 6. WHAM observations of the geocoronal hydrogen Balmer- α column emission during different solar conditions taken between December and the Spring equinox and in observing directions pointed toward very low Galactic emission regions of the sky. The data were taken during exceptional clear-sky conditions when the moon was not visible. The 1997 solar minimum (F10.7 69–76) data are from 10 nights of observations, the 2000 and 2001 near solar maximum data (F10.7 134–163) are from eight nights of observations, the 2004 solar medium data (F10.7 100–118) are from five nights of observations, and the 2008 observations are from two nights of observations (F10.7 69–70). The observations are the primary measurements, corrected for atmospheric extinction but not for tropospheric scattering. See text and Nossal et al. (2008) for discussion of uncertainties

fewer nights with more observations, and there are other bins where fewer spectra from more nights have been combined into a bin. The 1990 reanalyzed observations in Figures 3a and 3b are from one night with clear-sky conditions. Our review of the log notes and spectra indicates that clouds may have compromised observations from 1990 taken on other winter nights.

The observations taken by the WHAM included in Figure 4 were also plotted at a midrange shadow altitude of 2,783 km to facilitate their intercomparison. The WHAM observations included in this figure were taken during winter conditions and in viewing geometries pointed toward low Galactic emission regions. To extrapolate to facilitate comparison of observations when a data point was not present at an exact shadow altitude of interest, we fit a fifth-order polynomial to the log of the intensity plotted versus shadow altitude for each year of the WHAM winter data points. We then used the inverse log of this fit as the fit to the intensities from which we determined the intensity value at 2,783 km for each year. We used this method to reduce artificial undulations in the fit arising from uneven spacing of data points over the shadow altitude range (Nossal et al., 2012).

The black star at 1991 in Figure 4 is the original ratio of the observed to Anderson et al. (1987) solar maximum model intensity, normalized to 4.15 R. This data point corresponds to the right-most ratio in the top panel of Figure 6 of Nossal et al. (1993). To merge the pre-WHAM and WHAM data sets, we also used the fitting method applied to the WHAM observations in our reanalysis of the 1991 observations. We plotted the reanalyzed 1991 column emission inten-

sities versus shadow altitude as shown in Figures 3a and 3b and took the log of these intensities. We then fit a fifth-order polynomial to the log of these intensities to determine the fit and the corresponding intensity at a shadow altitude of 2,783 km. Superimposed on Figure 4 are these reanalyzed intensities for the 1991 observations at a shadow altitude of 2,783 using the value of 130 R for the R8 calibration (green circle), the calibration from the observation of the NAN during our best sky conditions during the summer months (purple circle), and the calibration value of 153 R for the R8 calibration (aqua circle).

Assessment of uncertainty becomes increasing difficult and of larger magnitude as we go backward in time. We used the scatter in the data to make an initial estimate of the *relative* uncertainty in the intensity. For the WHAM observations we calculated this *relative* uncertainty in the intensity to be ± 0.25 R. Additionally, there is a systematic $\pm 10\%$ uncertainty in the *absolute* intensity calibration, but this is a scaling factor for all of the WHAM data and does not affect the relative comparisons in intensity between WHAM observations. An estimate for the uncertainty for the *relative* intensity comparison for the 1990–1991 pre-WHAM observations is about ± 0.375 R based on scatter in the data. These uncertainties are included in the error bars in Figure 4. The reanalysis of the 1990–1991 observations indicated further uncertainty in the absolute intensity calibration of the R8 secondary calibration source. The impact of this uncertainty is described above and illustrated in the differences between the calculated intensities in Figures 3a and 3b and the points at 1991 in Figure 4. The earliest observations likely have higher uncertainty due to, for example, the lower sensitivity of the photomultiplier detection. Using scatter in the data, we have estimated the uncertainty in the *relative* intensity to be about ± 0.5 R for the 1980s data and the 1970s data.

Both the 4.15R normalization intensity and the WHAM intensities have been corrected for atmospheric extinction, but not for tropospheric scattering into the line of sight. As explained above, we used sensitivity studies to estimate contributions to uncertainties in the relative intensity comparison due to tropospheric scattering. Other sources of uncertainty are differences in viewing geometry and presence of Galactic emission. The WHAM observations included in this study were pointed toward low Galactic emission regions (≤0.6R; Nossal et al., 2008), and the pre-WHAM observations (Nossal et al., 1993) were taken in directions to avoid the Galactic plane to reduce the uncertainty due to the Galactic emission. We have included an

additional ± 0.25 R uncertainty for the 1970s, 1980s, and pre-WHAM 1990s column emission intensity observations; ± 0.15 R for the reanalysis 1990–1991 observations; and an additional ± 0.125 R uncertainty for the Wisconsin H-alpha Mapper intensities to more fully include the contributions of tropospheric scattering, Galactic emission, and other sources of uncertainty in the *relative* intensity comparison. Thus, our estimate of the combined uncertainties associated with the *relative* intensities for the 1970s and 1980s pre-WHAM observations is ± 0.75 R, for the 1990–1991 pre-WHAM observations is ± 0.625 R (original analysis) and ± 0.525 R (reanalysis), and for the WHAM observations is ± 0.375 R (see figure 4).

An additional analysis note is that when we reanalyzed the 1990 and 1991 original geocoronal and calibration spectra, the 1990 intensities were higher than those from 1991 (see Figures 3a and 3b) although the reverse was true in the original analysis (see black symbols in Figure 4). A contributing factor may be that in the reanalysis, the geocoronal spectral overlap was accounted for in determining the nebular calibration. Additionally, there may have been a few spectra included in the original analysis from nights where sky conditions were not pristine adding to scatter in the data. The solar F10.7 cm flux was higher for the 1990 observations than for the 1991 observations. In a future phase of reanalysis, fitting all of the pre-WHAM observations with the polynomial method used for the WHAM analysis and including observations in additional viewing geometries for some years with gaps in shadow altitude coverage could improve the accuracy of the comparison shown in Figure 4.

The solar radio flux at 10.7 cm over the period of our observations is plotted in Figure 5 as a proxy of solar activity and is higher during the Solar Cycle 22 maximum period of the 1990-1991 observations compared with conditions during the 2000-2001 near solar-maximum observations. These data were downloaded from the University of Colorado's Laboratory for Atmospheric and Space Physics (LASP) Interactive Solar Irradiance Datacenter (http://lasp.colorado.edu/lisird/data/noaa radio flux/). Also included on the LASP site are a composite solar Lyman α (121.6 nm) data set (http://lasp.colorado.edu/lisird/data/composite lyman_alpha/) including measurements from multiple instruments as discussed by Woods et al. (2000) and an empirical solar Lyman alpha model based on SOHO/SUMER observations (http://lasp.colorado. edu/lisird/data/lyman_alpha_model_ssi/; Kretzschmar et al., 2018). They show on the order of about 10% higher solar Lyman α during the 1990–1991 solar maxima period compared with the 2000–2001 period of our observations. More recent Lyman α observations by the SEE instrument (http://lasp.colorado.edu/ lisird/data/timed_see_lines_l3/) track closely with SEE Lyman β observations, though the solar Lyman β variation is of slightly larger amplitude over the solar cycle (http://lasp.colorado.edu/lisird/data/timed see lines 13/). However, these Lyman line observations are line integrated measurements, and it is the line center portion of the solar Lyman β emission that excites the geocoronal hydrogen Balmer- α line. There are few high-resolution measurements of the Lyman β line profile, adding uncertainty. If we assume that the SOHO/SUMER solar Lyman β line shape (Warren et al., 1998) measured during low solar activity is similar to that under high solar activity, an assumption made by Bishop et al. (2004), then we might expect that the line center solar Lyman β flux would also be higher during the 1990–1991 period.

5. Discussion

The observations presented here suggest an observed increase in the geocoronal hydrogen column emission intensity between the 1990–1991 solar maximum and the 2000–2001 near solar maximum periods, with the caveats that this is a limited data set and that there are uncertainties in the intensity calibration and other analysis factors. Agreement between the northern midlatitude observations from Pine Bluff, WI, and Kitt Peak Observatory during the same observing period suggests that the difference in intensity between the two solar maximum periods is likely not due to the observatory location.

An apparent increase in the hydrogen emission intensity between the 1990–1991 solar maximum period and the 2000–2001 near solar maximum period is counter to what we might expect given observations of the response of hydrogen Balmer- α column emission to changes in solar activity. Observations by the Wisconsin H-alpha Mapper Fabry-Perot during different solar conditions indicated a statistically significant solar cycle variation with observed intensities approximately 50% higher during solar maximum than during solar minimum conditions (Nossal et al., 2004, 2008, 2012). Figure 6 shows the solar cycle variation of the geocoronal hydrogen emission intensity observed by WHAM and plotted versus shadow altitude. This previous knowledge of the solar cycle influence would suggest that the hydrogen column emission intensities



would thus be higher during the Solar Cycle 22 observations, counter to what was observed. Further, the geocoronal hydrogen emission intensity during three solar minima was consistent within uncertainties, as illustrated in Figure 6 in Nossal et al. (2008).

The F10.7 cm flux range for the 1981 observations was roughly comparable to the range for the 1990–1991 observations as was the case for the 1982 observations, but some of the 1982 bin observations were taken during lower F10.7 conditions (see Figures 4 and 5). In this paper, we have chosen to focus on the comparisons between the 1990–1991 and 2000–2001 observations because we were able to refit and recalibrate the 1990–1991 original spectra, enhancing the accuracy of the comparison. Reviewing log notes for weather and pointing directions and calculating the shadow altitude with our current program should increase the accuracy of future comparisons with the 1970s and 1980s observations, even if the original spectra may not be available.

The apparent increase in the geocoronal hydrogen Balmer-α column emission intensity between two solar maximum periods is likely of larger magnitude than the response predicted by the NCAR onedimensional version of the Thermosphere Ionosphere Mesosphere Electrodynamics General Circulation Model. Simulation sensitivity experiments with this model predicted an increase of approximately 40% in the upper thermospheric hydrogen density in response to a doubling of carbon dioxide and methane at solar maximum as illustrated in Figures 5 and 6 in Nossal et al. (2016). Historical increases in methane and carbon dioxide, however, are about 150% and 40%, respectively, since 1750 (Intergovernmental Panel on Climate Change, 2013) and are within a few percent over the timescale of a solar cycle. The trend is more variable for methane than for carbon dioxide. Further, these simulations predicted that the hydrogen density would have a response to greenhouse gases of larger magnitude at solar minimum rather than at solar maximum conditions (Nossal et al., 2016). Future modeling with a three-dimensional model coupled to the troposphere that includes geographic, solar cyclic, seasonal, and diurnal information such as with the National Center for Atmospheric Research Whole Atmosphere Community Climate Model-eXtended (WACCM-X; Liu et al., 2018) should produce more accurate predictions for the thermospheric hydrogen response to greenhouse gas forcing, facilitating more accurate comparisons with observations.

The transport of solar Lyman β radiation is a nonlinear process including excitation via multiple scattering of hydrogen atoms within the Earth's shadow. Forward modeling with a radiative transfer code can be used to more accurately compare observations with model simulations by using the simulated density profiles coupled with the radiative transfer code to calculate intensities that would be observed from the ground (Gallant et al., 2019; Nossal et al., 2012). For the Gallant et al. (2019) and Nossal et al. (2012) studies, the NRLMSISE-00 model (Picone et al., 2002) was used to generate both the hydrogen density profile and the background thermosphere. The profile was extended upward using the analytic exospheric model of Bishop (1991). This model atmosphere was then coupled to the global resonance radiative transfer code of Bishop (1999) to calculate hydrogen Balmer α column emission intensities that would be observed from the ground. Future work using this forward modeling approach would facilitate more accurate comparisons between our observations and the WACCM-X model simulations of the response of hydrogen to solar variability and greenhouse gases.

Long-term observations with a single instrument at a clear air site would minimize uncertainties in the trend analysis and would be particularly beneficial if the instrument was at a location close to the mid-latitude sites of the previous observations. Taking calibration observations of multiple nebular sources on the same night, when possible, would aid in the intercalibration of secondary sources. Much of the year this is not possible when only one source is visible in the night sky. The approach used by Mierkiewicz et al. (2006) in which alternating observations of calibration sources and the geocorona are made with a stopped down field of view is useful for comparing calibrations of instruments with different fields of view as well as for taking observations of nebular regions with small fields of view to assess the uniformity of the intensity of the nebular calibration sources over the fields of view used for observations. The selection of a suite of Galactic observations for monitoring when taking terrestrial observations can corroborate the intensity calibration due to the invariance of the Galactic emission intensities. Additionally, geocoronal observational sequences can be designed to include those taken in directions of low Galactic emission and in the zenith directions throughout the night to facilitate comparisons with like viewing geometries.



6. Conclusions

We have used current analysis procedures to review and reanalyze geocoronal hydrogen emission observations and calibration spectra taken by the pre-WHAM Fabry-Perot interferometer from Wisconsin during the 1990–1991 period. Comparison of the 2000–2001 near-solar maximum geocoronal hydrogen Balmer- α emission observations with reanalysis of the 1990–1991 observations suggests an apparent increase in the hydrogen emission intensity between these two solar maximum and near-maximum periods, with the caveat that this is a limited data set and there are uncertainties in the calibration. This is a somewhat surprising result. This apparent increase in the hydrogen Balmer- α column emission intensity was not present in comparison of observations of the hydrogen column emission intensity from three solar minimum periods.

The data suggest the possibility of upper thermospheric hydrogen increases larger than would be expected due to current understanding of the response of hydrogen to solar cycle changes and increases in greenhouse gases. Solar activity was higher during the earlier solar maximum period. Thus, the apparent increase in intensity is counter to previous observations from Northern midlatitudes in which the observed intensity increases with higher solar activity. Additionally, the apparent increase in intensity is also likely of larger magnitude than would be consistent with model simulations of the response of upper thermopsheric hydrogen to increases in methane and carbon dioxide. Further, model simulations predict that a larger increase in thermospheric hydrogen due to increases in greenhouse gases would occur during solar minimum conditions.

The analysis of these observations provides guidance for optimizing future observational strategies regarding viewing geometry sequences and for including multiple approaches to corroborate the calibration. Comparisons of WHAM Southern Hemisphere observations and of future hydrogen emission observations during similar periods of the solar cycle would aid in corroborating the apparent increase in emissions in our Northern midlatitude observations and contribute to addressing the question of whether there are increases in hydrogen emissions of larger magnitude than would be predicted by model simulations of increases in greenhouse gases.

References

- Anderson, D. E. Jr., Meier, R. R., Hodges, R. R. Jr., & Tinsley, B. A. (1987). Hydrogen Balmer alpha intensity distributions and line profiles from multiple scattering theory using realistic geocoronal models. *Journal of Geophysical Research*, 92, 7619–7642. https://doi.org/10.1029/JA092iA07p07619
- Bishop, J. (1991). Analytic exosphere models for geocoronal applications. *Planetary and Space Science*, 39, 885–893. https://doi.org/10.1016/0032-0633(91)90093-P
- Bishop, J. (1999). Transport of resonant atomic hydrogen emissions in the thermosphere and geocorona: Model descriptions and applications. *Journal of Quantitative Spectroscopy & Radiative Transfer*, 61, 473–491. https://doi.org/10.1016/S0022-4073(98)00031-4
- Bishop, J. (2001). Thermospheric atomic hydrogen densities and fluxes from dayside Lyman α measurements. *Journal of Atmospheric and Solar Terrestrial Physics*, 63, 341–353. https://doi.org/10.1016/S1364-6826(00)00212-1
- Bishop, J., Harlander, J., Nossal, S., & Roesler, F. L. (2001). Analysis of Balmer α intensity measurements near solar minimum. *Journal of Atmospheric and Solar Terrestrial Physics*, 63(4), 341–353. https://doi.org/10.1016/S1364-6826(00)00212-1
- Bishop, J., Mierkiewicz, E. J., Roesler, F. L., Gómez, J. F., & Morales, C. (2004). Data-model comparison search analysis of coincident PBO Balmer alpha EURD Lyman beta geocoronal measurements from March 2000. *Journal of Geophysical Research*, 109, A05307. https://doi.org/10.1029/2003JA010165
- Brasseur, G., & Solomon, S. (2005). Aeronomy of the middle atmosphere. Dordrecht, Netherlands: Springer.
- Chamberlin, J. W., & Hunten, D. M. (1987). Theory of Planetary Atmospheres: An Introduction to their Physics and Chemistry (2nd ed.). New York: Elsevier.
- Coakley, M. M., Roesler, F. L., Reynolds, R. J., & Nossal, S. M. (1996). Fabry Perot CCD annular-summing spectroscopy: Study and implementation for aeronomy applications. Applied Optics, 35(33), 6479–6493. https://doi.org/10.1364/AO.35.006479
- Ehhalt, D. H. (1986). On the consequence of tropospheric CH4 increase to the exospheric density. *Journal of Geophysical Research*, 91, 2843. https://doi.org/10.1029/JD091iD02p02843
- Emmert, J. T. (2015). Altitude and solar activity dependence of 1967–2005 thermospheric density trends derived from orbital drag. *Journal of Geophysical Research: Space Physics*, 120, 2940–2950. https://doi.org/10.1002/2015JA021047
- Emmert, J. T., Picone, J. M., Lean, J. L., & Knowles, S. H. (2004). Global change in the thermosphere: Compelling evidence of a secular decrease in density. *Journal of Geophysical Research*, 109, A02301. https://doi.org/10.1029/2003JA010176
- Gallant, M. A., Mierkiewicz, E. J., Nossal, S. M., Qian, L., Burns, A. G., Zacharias, A. R., & Roesler, F. L. (2019). Signatures of thermospheric-exospheric coupling of hydrogen in observed seasonal trends of H α intensity. *Journal of Geophysical Research: Space Physics*, First published, 22 April124, 4525–4538. https://doi.org/10.1029/2018JA026426
- Gardner, D. D., Mierkiewicz, E. J., Roesler, F. L., Harlander, J. M., Jaehnig, K. P., Nossal, S. M., & Haffner, L. M. (2017). First performance results of a new field-widened spatial heterodyne spectrometer for geocoronal Hα research. *Journal of Geophysical Research: Space Physics*, 121, 1373–1385. https://doi.org/10.1002/2016JA022625
- Gardner, D. D., Mierkiewicz, E. J., Roesler, F. L., Nossal, S. M., & Haffner, L. M. (2017). Constraining Balmer alpha fine structure excitation measured in geocoronal hydrogen observations. *Journal of Geophysical Research: Space Physics*, 122, 10,727–10,747. https://doi.org/ 10.1002/2017JA024055

Acknowledgments

We are grateful to Ron Reynolds for invaluable discussions regarding the intensity calibration. We also thank Jeff Percival for the development and our use of his code to calculate the shadow altitude associated with our observations and Grant Petty for collaboration on the development of a tropospheric scattering correction code and the use of his Monte Carlo radiative transfer code. Additionally, we thank Arianna Ranabhat and Nikaan Koupaei Abyazani for contributions to the analysis of the WHAM data. We also appreciate helpful discussions about this work with Stan Solomon and the thoughtful suggestions provided by the reviewers. We are grateful for the support provided by the National Science Foundation Grants AGS-1343048 and AGS-1352311. Support for this research was also provided by the University of Wisconsin-Madison Office of the Vice Chancellor for Research and Graduate Education with funding from the Wisconsin Alumni Research Foundation. WHAM observations and operations in Chile have been supported by National Science Foundation Awards AST-1108911 and AST-1714472/1715623. Data are on the following Zenodo repository (DOI: 10.5281/ zenodo.3515451). We have also created a github repository (https://github. com/smnossal/Hemissiondata) that links to this Zenodo repository and where we can post updates to the data



- Haffner, L.M. Reynolds, R.J., Babler, B.L., Madsen, G.J., Hill, A.S., Barger, K., et al., (2016), The Wisconsin HAlpha Mapper Sky Survey; American Astronomical Society Meeting Abstracts# 227, 2016
- Haffner, L. M.; Reynolds, R. J.; Madsen, G. J.; Hill, A. S.; Barger, K. A.; Jaehnig, K. P.; et al. (2010), Early results from the Wisconsin H-Alpha Mapper Southern Sky Survey Volume: 438, The Dynamic Interstellar Medium: A Celebration of the Canadian Galactic Plane Survey, p. 388.
- Haffner, L. M., Reynolds, R. J., Tufte, S. L., Madsen, G. J., Jaehnig, K. P., & Percival, J. W. (2003). The Wisconsin H-alpha mapper northern sky survey. *Astrophysical Journal Supplement Series*, 149(2), 405–422. https://doi.org/10.1086/378850
- Intergovernmental Panel on Climate Change (2013). Climate change 2013: The physical science basis, in contribution of Working Group I to the Fifth Assessment Report of the Intergovernmental Panel on Climate Change, edited by T. F. Stocker et al., Cambridge University Press, Cambridge, U. K., and New York.
- Kerr, R. B., Garcia, R., He, X., Noto, J., Lancaster, R. S., Tepley, C. A., et al. (2001a). Periodic variations of geocoronal Balmer α brightness due to solar driven exospheric abundance variations. *Journal of Geophysical Research*, 106(A12), 28,797–28,817. https://doi.org/10.1029/
- Kerr, R. B., Garcia, R., He, X., Noto, J., Lancaster, R. S., Tepley, C. A., et al. (2001b). Secular variability of the geocoronal Balmer α brightness: Magnetic activity and possible human influences. *Journal of Geophysical Research*, 106(A12), 28,819–28,830. https://doi.org/10.1029/1999JA900187
- Krall, J., Glocer, A., Fok, M.-C., Nossal, S. M., & Huba, J. D. (2018). The unknown hydrogenexosphere: Space weather implications. Space Weather, 16, 205–215. https://doi.org/10.1002/2017SW001780
- Kretzschmar, M., Snow, M., & Curdt, W. (2018). An empirical model of the variation of the solar Lyman-α spectral irradiance. *Geophysical Research Letters*, 45, 2138–2144. https://doi.org/10.1002/2017GL076318
- Liu, H.-L., Bardeen, C. G., Foster, B. T., Lauritzen, P., Liu, J., Lu, G., et al. (2018). Development and validation of the whole atmosphere community climate model with thermosphere and ionosphere extension (WACCM-X v. 2.0). *Journal of Advances in Modeling Earth Systems*, 10, 381–402. https://doi.org/10.1002/2017MS001232
- Mierkiewicz, E. J. (2002). Fabry-Perot observations of the hydrogen geocorona (PhD thesis). Univ. of Wisc.-Madison, Madison.
- Mierkiewicz, E. J. (2019). Neutral hydrogen in the terrestrial thermosphere and exosphere: A ground-based perspective, accepted as a chapter in the AGU centennial book, Advances in Upper Atmosphere Research: Dynamics and Energetics.
- Mierkiewicz, E. J., Roesler, F. L., & Nossal, S. M. (2012). Observed seasonal variations iexospheric effective temperatures. *Journal of Geophysical Research*, 117, A06313. https://doi.org/10.1029/2011JA017123
- Mierkiewicz, E. J., Roesler, F. L., Nossal, S. M., Bishop, J., Reynolds, R. J., & Haffner, L. M. (2006). Geocoronal hydrogen studies using Fabry-Perot interferometers. Part 1: Instrumentation, observations, and analysis. *Journal of Atmospheric and Solar-Terrestrial Physics*, 68, 1520–1552. https://doi.org/10.1016/j.jastp.2005.08.024
- Nossal, S., Reynolds, R. J., Roesler, F. L., & Scherb, F. (1993). Solar cycle variations of geocoronal Balmer α emission. *Journal of Geophysical Research*, 98, 3669–3676. https://doi.org/10.1029/92JA02568
- Nossal, S., Roesler, F. L., Reynolds, R. J., Haffner, M., Tufte, S., Bishop, J., & Percival, J. (2001). Geocoronal Balmer α intensity measurements using the WHAM Fabry-Perot facility. *Journal of Geophysical Research*, 106, 5605–5616. https://doi.org/10.1029/2000JA000003
- Nossal, S. M., Mierkiewicz, E. J., & Roesler, F. L. (2012). Observed and modeled solar cycle variation in geocoronal hydrogen using NRLMSISE-00 thermosphere conditions and the Bishop analytic exosphere model. *Journal of Geophysical Research*, 117, A03311. https://doi.org/10.1029/2011JA017074
- Nossal, S. M., Mierkiewicz, E. J., Roesler, F. L., Haffner, L. M., Reynolds, R. J., & Woodward, R. C. (2008). Geocoronal hydrogen observations spanning three solar minima. *Journal of Geophysical Research*, 113, A11307. https://doi.org/10.1029/2008JA013380
- Nossal, S. M., Mierkiewicz, E. J., Roesler, F. L., Reynolds, R. J., & Haffner, L. M. (2006). Geocoronal hydrogen studies using Fabry-Perot interferometers, Part 2: Long term observations. *Journal of Atmospheric and Solar Terrestrial Physics*, 68, 1553–1575. https://doi.org/10.1016/j.jastp.2005.08.025
- Nossal, S. M., Qian, L., Solomon, S. C., Burns, A. G., & Wang, W. (2016). Thermospheric hydrogen response to increases in greenhouse gases. *Journal of Geophysical Research: Space Physics*, 121, 3545–3554. https://doi.org/10.1002/2015JA022008
- Nossal, S. M., Roesler, F. L., Mierkiewicz, E. J., & Reynolds, R. J. (2004). Observations of solar cyclic variations in geocoronal Hα column emission intensities. *Geophysical Research Letters*, 31, L06110. https://doi.org/10.1029/2003GL018729
- Percival, J. W., A software state machine for computing astronomical coordinates. Astronomical Data Analysis Software and Systems III A. S.P Conference Series, Vol 61, 1994, p 477, 1994ASPC..61..477P
- Petty, G. W. (2002). Area-average solar radiative transfer in three-dimensionally inhomogeneous clouds: The Independently Scattering Cloudlet model. *Journal of the Atmospheric Sciences*, 59, 2910–2929.
- Petty, G. W. (2006). A first course in atmospheric radiation (2nd ed., p. 460). Madison, WI: Sundog Publishing. ISBN-13: 978-0-9729033-1-8 Picone, J. M., Hedin, A. E., & Drob, D. P. (2002). NRLMSISE-00 empirical model of the atmosphere: Statistical comparisons and scientific issues. Journal of Geophysical Research, 107(A12), 1468. https://doi.org/10.1029/2002JA009430
- Qian, L., Burns, A. G., Solomon, S. S., Smith, A. K., McInerney, J. M., Hunt, L. A., et al. (2018). Temporal variability of atomic hydrogen from the mesopause to the upper thermosphere. *Journal of Geophysical Research: Space Physics*, 123, 1006–1017. https://doi.org/10.1002/20171A024998
- Qian, L., Laštovička, J., Roble, R. G., & Solomon, S. C. (2011). Progress in observations and simulations of global change in the upper atmosphere. *Journal of Geophysical Research*, 116, A00H03. https://doi.org/10.1029/2010JA016317
- Qin, J., & Waldrop, L. (2016). Non-thermal hydrogen atoms in theterrestrial upper thermosphere. *Nature Communications*, 7, 13655. https://doi.org/10.1038/ncomms13655
- Roble, R. G., & Dickinson, R. E. (1989). How will changes in carbon dioxide and methane modify the mean structure of the mesosphere and thermosphere? *Geophysical Research Letters*, 16, 1441–1444. https://doi.org/10.1029/GL016i012p01441
- Roesler, F. L. (1974). Fabry-Perot instruments of astronomy. In Methods of Experimental Physics, vol. 12A, Astrophysics, Part A: Optical and Infrared (pp. 531–569). New York: Academic.
- Roesler, F. L., Mierkiewicz, E. J., & Nossal, S. M. (2014). The geocoronal Hα cascade component determined from geocoronal Hβ intensity measurements. *Journal of Geophysical Research: Space Physics*, 119, 6642–6647. https://doi.org/10.1002/2014JA020026
- Roesler, F. L., Reynolds, R. J., & Scherb, F. (1995). Fabry-Perot spectroscopy of extremely faint astronomical sources, tridimensional optical spectroscopic methods in astrophysics, ASP conference series, Volume 71. Proceedings of I.A.U. Colloquium 149, held in Marseille, France. March 22-25. 1994. Editor(s). G. Comte. M. Marcelin. Astronomical Society of the Pacific.
- Scherb, F. (1981). Hydrogen production rates from ground-based Fabry-Perot observations of comet Kohoutek. *Astrophysical Journal*, 243, 644–650.



10.1029/2019JA026903



- Solomon, S. C., Liu, H.-L., Marsh, D. R., McInerney, J. M., Qian, L., & Vitt, F. M. (2018). Whole atmosphere simulation of anthropogenic climate change. *Geophysical Research Letters*, 45, 1567–1576. https://doi.org/10.1002/2017GL076950
- Tinsley, B. A., Hodges, R. R. Jr., & Rohrbaugh, R. P. (1986). Monte Carlo models for the terrestrial exosphere over a solar cycle. *Journal of Geophysical Research*, 91(A12), 13,631–13,647. https://doi.org/10.1029/JA091iA12p13631
- Warren, H. P., Mariska, J. T., & Wilhelm, K. (1998). High-resolution observations of the solar hydrogen Lyman lines in the quiet sun with the SUMER instrument on SOHO. *The Astrophysical Journal Supplement Series*, 119(1), 105–120. https://doi.org/10.1086/313151
- Woods, T. N., Tobiska, W. K., Rottman, G. J., & Worden, J. R. (2000). Improved solar Lyman α irradiance modeling from 1947 through 1999 based on UARS observations. *Journal of Geophysical Research*, 105(A12), 27,195–27,215. https://doi.org/10.1029/2000JA000051